ISIJ International, Vol. 60 (2020), No. 9, pp. 1985–1992

Industrial Ladle Furnace Slag Composition Analysis with Optical Emissions from the Arc

Henri PAUNA,[1)]* Matti AULA,[1)] Jonas SEEHAUSEN,[2)] Jens-Sebastian KLUNG,[2)] Marko HUTTULA[3)] and Timo FABRITIUS[1)]

1) Process Metallurgy Research Group, University of Oulu, P.O. Box 4300, Oulu, FI-90014 Finland.
2) Deutsche Edelstahlwerke, Obere Kaiserstraße, Siegen, 57078 Germany.
3) Nano and Molecular Systems Research Unit, University of Oulu, P.O. Box 3000, Oulu, FI-90014 Finland.

(*Received on October 29, 2019; accepted on February 14, 2020; J-STAGE Advance published date: April 1, 2020*)

With the strict standards for steel quality and high production rates, the demand for faster and more convenient slag composition analysis for both electric arc and ladle furnaces has become a major issue in industrial steel plants. To overcome the time-delay between slag sampling and results of the slag composition analysis, an on-line slag composition analysis is required. Such a method that can be used in on-line analysis and is also chemically sensitive to the slag composition is optical emission spectroscopy. In this work, the optical emissions from the arc have been measured in an industrial ladle furnace and used for slag composition analysis. This article focuses on CaF_2 and MgO, since the CaF_2 is a common additive material in the ladle treatment and high MgO content means that the ladle refractory lining is dissolving into the slag. The analysis has been carried out by comparing emission line ratios to the XRF analyzed ratios of CaF_2/MgO and MnO/MgO, respectively. The results show that several atomic emissions lines of calcium, magnesium, and manganese can be used to evaluate the CaF_2/MgO and MnO/MgO ratios in the slag. It was found out that the plasma temperature derived from Ca I emission lines has a non-linear relation with the CaF_2 content of the slag. Additionally, the dissociation pathways of molecular slag components were determined and studied in different plasma temperatures with equilibrium composition computation in order to determine the relations between the slag and plasma compositions.

KEY WORDS: ladle furnace; optical emission spectroscopy; slag composition; on-line analysis; plasma analysis.

1. Introduction

Ladle furnaces (LFs) are used to fine-tune the chemical composition of the steel before casting. The impurities from the steel are accumulated to slag that floats on top of the molten steel due to density difference. The slag has an important role in steelmaking, since the nonmetallic impurities can cause harmful inclusions into the steel.[1)] The viscosity and inclusions are usually modified by additive materials, such as CaF_2 and CaO. The main components of the LF slags are the compounds of calcium, silicon, magnesium, and aluminum,[2)] with varying amounts of sulphur,[3–6)] manganese,[7,8)] and other minor impurities. Also traces of chromium and iron might transfer from the steel into the slag.

In the electric steelmaking, the electric arc furnace (EAF) and LF slags are quantitatively a major by-product.[9)] The slag itself can have many applications, such as cement material[10,11)] or as a flux in the steel industry.[12)] Due to the high production rate and usability of the slags, the valorization of slags has gained a lot of interest in the steel industry.[11,13)] The main problem in the usage of slags is the varying composition of the slag, which has an impact on the behavior and effects of the product.[9)] Thus, the knowledge of the slag composition has a key role in its usage and recycling.

A common way to determine the slag composition at ladle furnaces is to do an x-ray fluorescence (XRF) analysis.[12)] The XRF analysis consists of slag sampling, grinding, and spectral analysis at *e.g.* a nearby laboratory. However, there is a delay between the sampling and obtaining the XRF results due to careful sample preparation and XRF analysis.[14)] At this point, the ladle treatment might already be finished, and the XRF results can only be used to prepare for the next melt instead of affecting the ongoing operations. Various models have been made to predict the steel and slag composition,[14–16)] but feasible analytical on-line methods for slag composition analysis have not yet been developed.

As an additive material in steelmaking, CaF_2 usually decreases the viscosity of the slag.[7,8,17–20)] This is especially notable with slags containing SiO_2.[8,20)] CaF_2 has also been observed to affect the crystallization temperature of the slags[7,8,18)] and the activity coefficient of FeO.[21)] On the other hand, in high MnO concentrations it is not recommended

* Corresponding author: E-mail: henri.pauna@oulu.fi
DOI: https://doi.org/10.2355/isijinternational.ISIJINT-2019-676

to add large amounts of CaF_2 due to corrosion of refractory material.[8] Due to the apparent effect of CaF_2 to the properties of the slag, it is very important to adjust the CaF_2 addition levels to optimized range.

From the refractory lining lifetime point of view, MgO content of the slag has to be monitored. In some cases, even though magnesium is not added during the LF treatment, MgO is found from the slag. Jia *et al.* observed that inclusions contained magnesium in aluminum killed steel even though no magnesium was added and concluded that the magnesium might dissolve from the refractory of the furnace or come via reactions between the slag and steel.[22] The slag composition can be used to determine whether or not the slag is saturated with respect to the MgO, *i.e.* is there a driving force for the refractory to be dissolved into the melt. Hence, MgO content in the slag can be used to evaluate the refractory wear and make adjustments to the slag in order to prevent the dissolution of the refractory.

Optical emission spectroscopy (OES) is a method with which the atomic and molecular optical emissions of a substance can be measured. Since the atomic and molecular structure of each species is unique, this method can be used to determine the chemical composition of a substance. The prospects of OES analysis for Cr_2O_3 content of the EAF slag have already been realized with prospects of on-line slag composition analysis capability[23] in addition to process control characterization.[24] The same measurement procedure, including only the spectrometer equipment and data analysis computer, can also be utilized in ladle furnaces.

In this work, the CaF_2 content together with CaF_2/MgO and MnO/MgO ratios in industrial ladle furnace slags have been analyzed with OES and plasma diagnostics with the optical emissions from the electric arc. The results of the OES analysis have been correlated with XRF slag composition analysis results. Since CaF_2 is a common additive material in the ladle treatment, the amount of CaF_2 could be fine-tuned with on-line OES analysis. As a reference point, MgO is a suitable and interesting species, since it is not always naturally present in the ladle slag but can be dissolved from the furnace lining into the slag.

2. Methods and Materials

The measurement campaign was conducted at an industrial 140 t LF in Deutsche Edelstahlwerke (DEW), Germany. The on-site OES measurement equipment consisted of three spectrometers covering ultraviolet (UV), visible (VIS), and near infra-red (NIR) wavelength ranges, and a data storage computer. The spectrometers were Czerny-Turner Avaspec-ULS2048 provided by Luxmet Oy. The UV, VIS, and NIR spectrometers covered 247.337–419.199 nm, 298.267–866.400 nm, and 496.655–1 048.934 nm, respectively. The spectral resolutions of the spectrometers were 0.05 nm for the UV and 0.15 nm for the VIS and NIR. Three spectrometers with different wavelength ranges were used in order to cover as much of the spectral range of the atomic arc emissions as possible. The light from the arc was collected with three optical fibers that guided the light to the spectrometers. The optical fibers were attached to a measurement head which was placed several meters away from the furnace ensuring a totally safe environment for the equipment. The optical fibers were protected with a tube and a pressurized airflow through the tube prevented any slag splashes from hitting the measurement head. The fibers looked into the furnace through a gap between the ladle and the furnace roof. A schematic image of the measurement set-up is presented in **Fig. 1**. The OES data was analyzed on a separate computer with Matlab-based self-developed software after the measurement campaign.

In the DEW LF campaign, ladles were switched frequently. The view cone into the different ladles remained the same, but each ladle had a chance to have accumulated slag that blocked the view into the furnace. Thus, all of the melts were not measurable by the OES. Visual inspection on site proved that this was caused by clogged view cone into the furnace. By taking into account the occasionally blocked view into the furnace and varying heights of the furnace roof and the slag surface, roughly half of the melts were analyzable by the OES. However, on site tests showed that if the roof is raised for even a short period of time, the optical emissions from the arc can be measured. The accumulated slag that blocks the view into the furnace, on the other hand, could be crushed before the ladles are switched to provide a better view into the furnace. These procedures were not deployed in this measurement campaign.

The measurement campaign was separated into two parts. The first part was performed with only the plain fibers that collected the light, whereas in the second part a light gath-

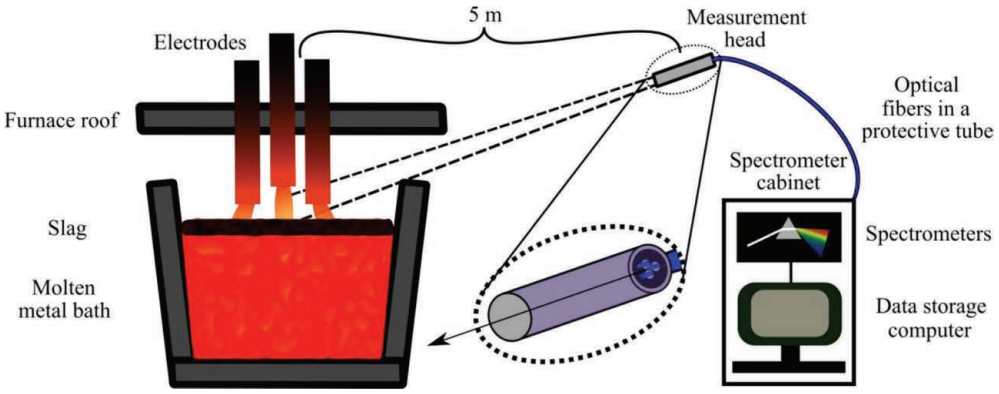

Fig. 1. Schematic presentation of the measurement set-up at the DEW LF. The view cone of the measurement head into the furnace has been marked with dashed lines. The direction of the pressurized airflow has been marked with an arrow. (Online version in color.)

ering lens was adjusted in front of the measurement head in order to increase the light intensity. The main reason for adding the lens to the set-up was to increase the intensity of the UV light. In an industrial LF, the UV light is efficiently absorbed by the furnace atmosphere and evaporated material. In our tests at laboratory and pilot-scale EAFs, on the other hand, we have acquired emission lines also from the range of 240–350 nm without the lens. In this work, the UV spectra have been acquired with the lens, whereas VIS and NIR without the lens. Example spectra for UV, VIS, and NIR are presented in **Fig. 2**. All of the spectra that were used in the analysis were recorded 5–30 minutes before the end of each melt depending on the conditions inside the furnace.

The XRF data analyses were made as a standard procedure of ordinary ladle treatment at the steel plant for slag samples that were taken before degassing. In the OES analysis, the intensities of the calcium or manganese emission lines were divided by those of the magnesium emission lines in order to correlate the OES data to the XRF analyzed CaF_2/MgO and MnO/MgO ratios in the slag. Additionally, this method removes the effect of varying overall intensity of the spectra. When several emission lines of calcium are divided by the same reference line of magnesium, the data sets of different calcium emission lines can be combined. Each line ratio is first normalized across all of the measured melts by dividing each data point with the maximum value of the line ratios. Then, for each melt, an average of these normalized values for the different calcium lines is used as the final data point for the slag composition analysis. When the trends of the emission lines are similar, this procedure usually results into a more accurate interpretation of the correlation between the OES and XRF. This method has been used in this study for several calcium lines.

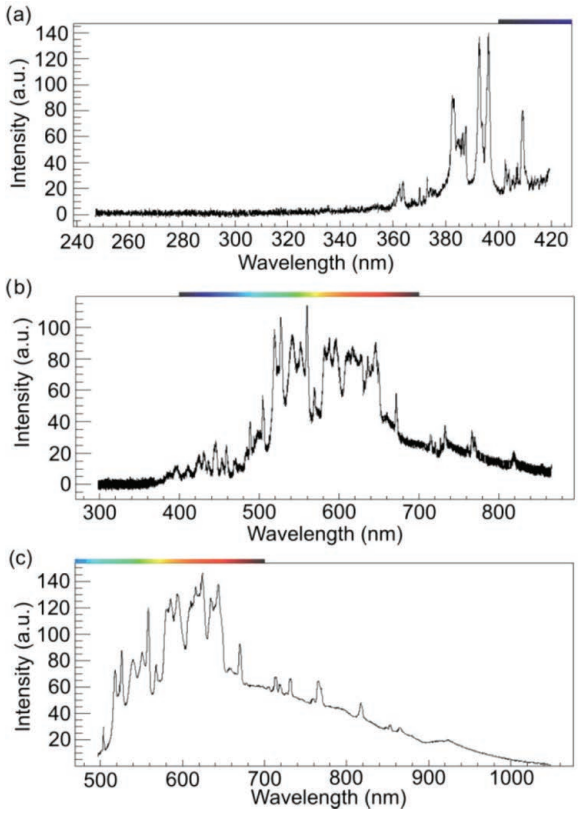

Fig. 2. Emission spectra from the arc for (a) UV, (b) VIS, and (c) NIR. The UV spectrum has been measured with the lens, whereas the VIS and NIR spectra without the lens. (Online version in color.)

3. Theoretical

According to the work of C. Aragón and J. A. Aguilera, the plasma temperature can be determined using the Boltzmann plot with OES data.[25] The Boltzmann plot equation is

$$ln\left(\frac{\varepsilon^z \lambda_{mn}}{g_m A_{mn}}\right) = -\frac{1}{kT}E_m^z + ln\left(\frac{hcN^z}{4\pi U^z(T)}\right) \quad \text{..... (1)}$$

in which z is the ionization state, ε is the wavelength-integrated emissivity, λ is the emission line wavelength, subscripts n and m are the lower and upper energy levels, respectively, g is the degeneracy of the energy level, k is the Boltzmann constant, T is the temperature, and E is the energy of the energy level. The term in the far right including the Planck's constant h, speed of light c, number density N, and partition function $U^z(T)$, can be neglected because it is constant at a given temperature and hence does not contribute to the slope of the Boltzmann plot. ε, on the other hand, is proportional to the intensity of the emission line, assuming that the plasma is in local thermodynamic equilibrium (LTE).[25]

Saha-Boltzmann equation has been used to determine the electron density of the plasma.[25] When the correction term of ionization energy, which has insignificant effect to the electron density in the scope of this work, is neglected, the Saha-Boltzmann equation is

$$N_e = C\sqrt{T^3}\,\frac{I_{mn}^z \lambda_{mn}^z A_{ij}^{z+1} g_i^{z+1}}{I_{ij}^{z+1} \lambda_{ij}^{z+1} A_{mn}^z g_m^z}\, exp\left(\frac{E_m^z - E_{ion} - E_i^{z+1}}{kT}\right) \quad \text{..... (2)}$$

in which C is $2(2\pi m_e k)^{3/2}/h^3$, m_e is the mass of electron, I^z is the intensity of emission line, and E_{ion} is the ionization energy of the ground state.

Fulfillment of the LTE condition has been evaluated with the McWhirter criterion[25,26]

$$N_e \geq 1.6\times10^{12}\sqrt{T}(\Delta E)^3\ cm^{-3} \quad \text{..... (3)}$$

in which ΔE is the energy difference between energy levels in electron volts and T is the temperature in Kelvins. The

Table 1. Ca I and Ca II emission line wavelengths λ (nm), transition probabilities A_{ij} (s^{-1}), upper and lower level energies E_i and E_j (eV), respectively, and upper level degeneracy g_i.

Plasma T	λ	A_{ij}	E_j	E_i	g_i
Ca I	518.885	4.0E+07	2.933	5.321	5
Ca I	526.424	9.1E+06	2.523	4.878	5
Ca I	558.197	6.0E+06	2.523	4.744	7
Ca I	560.285	1.4E+07	2.523	4.735	3
Plasma N_e	λ	A_{ij}	E_j	E_i	g_i
Ca I	504.162	3.3E+07	2.709	5.168	3
Ca II	396.847	1.4E+08	0.000	3.123	2
Plasma LTE	λ	A_{ij}	E_j	E_i	g_i
Ca I	504.162	3.3E+07	2.709	5.168	3

McWhirter criterion states that the rate of collisional processes is at least ten times the rate of radiative processes, thus ensuring a more uniform energy distribution.[26] The emission lines that have been used in the plasma temperature, density, and criterion density analysis are listed in the **Table 1**. The attenuations of these emission lines due to varying spectrometer transmittance did not have significant effect to the intensities of the lines. Emission line specific constants have been acquired from the NIST Atomic Spectra Database.[27]

4. Results and Discussion

The data from the measurements without the lens was used to analyze the VIS and NIR spectra. The light acquisition from the electric arc is easier for visible and longer wavelengths than for UV, since the UV light tends to be absorbed by *e.g.* the furnace atmosphere. In the beginning of the measurement campaign it was plain to see that the VIS and NIR spectrometers received enough light for the OES analysis, whereas the UV spectrometer showed nothing but minor background radiation. The installation of the lens allowed to obtain UV spectra above 300 nm. Below 300 nm, most of the light from the arc gets absorbed and thus the weak lines were not observable. The increased intensity between 300 and 420 nm, however, allowed to identify emission lines of calcium, magnesium, and manganese.

The emission lines for calcium, magnesium, and manganese that were used for the CaF_2/MgO and MnO/MgO correlation analysis are listed in **Table 2** for UV, VIS, and NIR. 10 Ca I, 1 Ca II, 7 Mg I, and 1 Mn I lines were found to be suitable for the slag composition analysis. Different Ca I lines were used for the VIS and NIR spectra in order to increase the number of suitable emission line candidates. Ca I 4 is one of the few emission lines of calcium that has practically no overlap with nearby emission lines in the LF spectra, whereas the other Ca I lines have some overlap with neighbouring lines. Furthermore, the spectra from an industrial LF do not always reach the quality of for example pilot-scale EAF spectra.[28] The effect of error from the overlap has been minimized by fitting all the emission lines corresponding to emissions also from the slag components other than calcium, magnesium, and manganese.

The correlations between CaF_2/MgO or MnO/MgO and Ca I/Mg I or Mn I/Mg O, respectively, have been presented in the **Figs. 3**, **4**, and **5** for the emission lines listed in the

Table 2. Calcium and magnesium emission lines used for UV, VIS, and NIR CaF_2/MgO and MnO/MgO analysis.

Species	#	Wavelength (nm)	UV	VIS	NIR
Ca I	1	387.578	x		
	2	395.705	x		
	3	397.371	x		
	4	504.162		x	x
	5	526.424			x
	6	527.036			x
	7	558.197		x	
	8	558.876		x	
	9	559.447		x	
	10	560.285		x	
Ca II	1	409.719	x		
Mg I	1	382.935	x		
	2	383.230	x		
	3	383.829	x		
	4	392.647	x		
	5	516.732		x	x
	6	517.268		x	x
	7	518.360		x	x
Mn I	1	403.076	x		

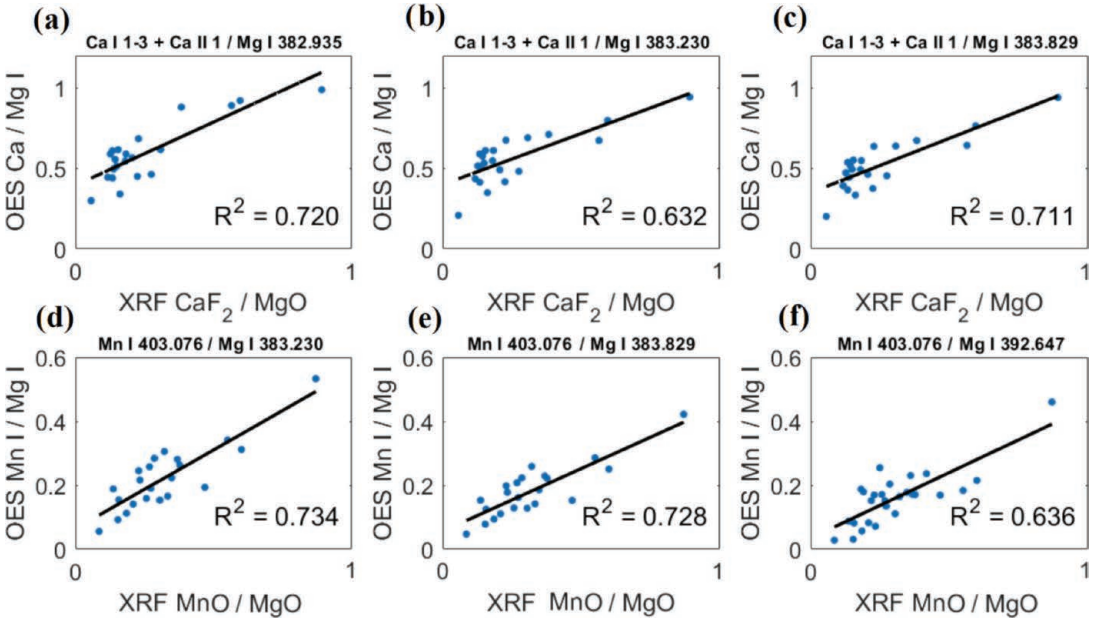

Fig. 3. Correlation between the XRF and OES analysis between CaF_2/MgO and Ca I/Mg I together with MnO/MgO and Mn I/Mg I for UV spectra. (a)–(c) include 21 melts, (d) and (e) 22 melts, and (f) 27 melts. The calcium line numbers refer to the # in Table 2. The XRF axes have been normalized. (Online version in color.)

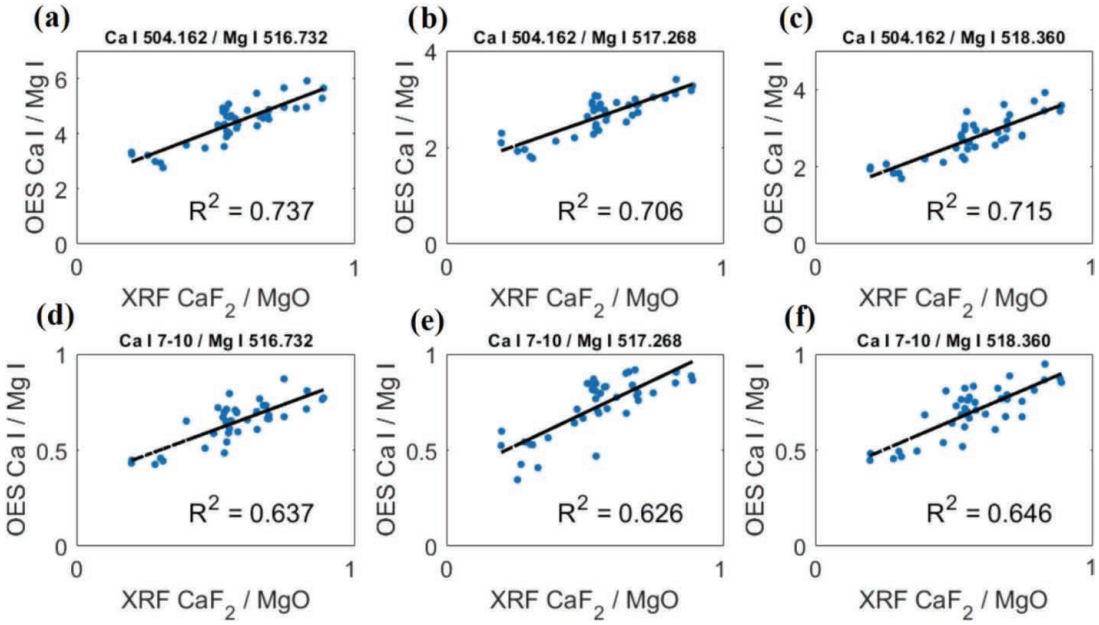

Fig. 4. Correlation between the XRF and OES analysis between CaF_2/MgO and Ca I/Mg I emission lines, respectively, for VIS spectra. (a), (e), and (f) include 40 melts, (c) 39 melts, and (b) and (d) 38 melts. The calcium line numbers refer to the # in Table 2. The XRF axes have been normalized. (Online version in color.)

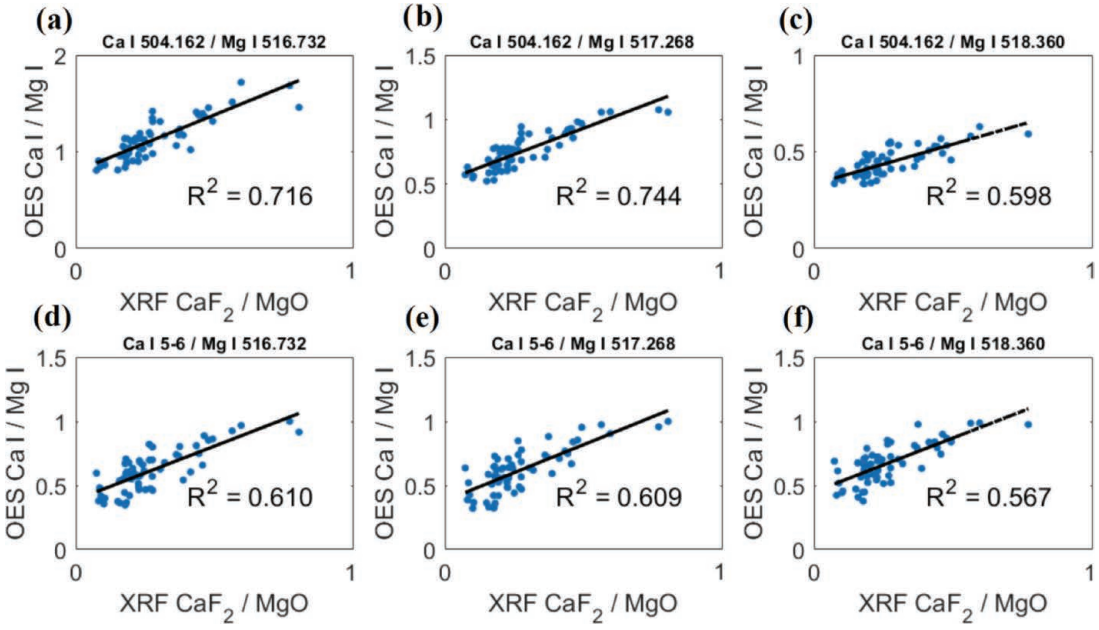

Fig. 5. Correlation between the XRF and OES analysis between CaF_2/MgO and Ca I/Mg I emission lines, respectively, for NIR spectra. (a), (b), (d), and (e) include 60 melts, and (c) and (f) 59 melts. The calcium line numbers refer to the # in Table 2. The XRF axes have been normalized. (Online version in color.)

Table 2. The XRF axes for the CaF_2/MgO and MnO/MgO ratios have been normalized. The UV, VIS, and NIR emission line ratios show similar results towards the CaF_2/MgO correlation. In the VIS and NIR spectra, the best correlations are found for the most isolated Ca I 4 emission line. Ca I 5–10 lines overlap with neighbouring emission lines and thus have uncertainty included. The correlation of Ca I lines 5–10 were improved by combining the line ratios through normalization and averaging, so that VIS analysis combined Ca I lines 7–10 and NIR Ca I lines 5–6. For the UV correlations, Ca I 1–3 and Ca II 1 were combined with similar procedure. In order to improve the correlation of individual Ca I emission lines in future campaigns at LFs, the measurement head might have to be relocated to ensure an even better view cone into the electric arc. This could reduce the effect of light reflections and increase the light intensity.

The VIS spectra showed a static disturbance throughout the spectra, which was most probably caused by either the spectrometer configurations or a malfunction in the spectrometer. This can be seen in the Fig. 2(b) in the lower and upper wavelength ranges where mostly the background radiation is observed. Hence, the VIS spectra were not as accurate in higher CaF_2 concentrations when compared to the NIR spectra. The lower ratio of Ca I/Mg I in Fig. 5 when compared to Fig. 4 for Ca I 4 line occurs because the line is near to the lower limit of the NIR spectral range, at

which point the transmission of the spectrometer is lower than in the center of the wavelength range.

As can be seen from the Figs. 4 and 5, the coefficient of correlation, R^2, is highest for the Ca I 4 emission line for the VIS and NIR. The R^2 values of the combined Ca I line ratios of the VIS and NIR, on the other hand, are below 0.70. With these spectrometer configurations, the emission lines that would be used for the slag composition evaluation have to be very carefully selected and calibrated with the XRF composition results. Furthermore, Ca I 4 line ratios had the most melts included because the line is isolated and hence is not as prone to uncertainty as the other Ca I lines. The most melts were included in the NIR analysis due to higher sensitivity of the NIR spectrometer, whereas the VIS analysis included up to 40 melts due to lower sensitivity. In this study, the visible range of the NIR spectra provided the most accurate correlation between the XRF and OES.

Electron density N_e and LTE criterion density were determined with Eqs. (2) and (3) with the Ca I and Ca II lines listed in the Table 1 using the VIS spectra. The electron density varied between 1.70×10^{18} and 7.00×10^{19} cm^{-3} and the LTE criterion density between 1.20×10^{15} and 2.00×10^{15} cm^{-3}. Thus, the electron density always exceeded the criterion density for LTE by several magnitudes.

It was noted in a previous work on pilot-scale EAF that the plasma temperature, especially for calcium, is strongly affected by the slag composition.[28] In the present work, it was found out that the CaF_2 content in the slag correlates with the plasma temperature that was determined with the Ca I lines in the Table 1 using Eq. (1). This correlation is presented in the **Fig. 6** for 78 melts. The equation describing the correlation between the CaF_2 content of the slag and plasma temperature is

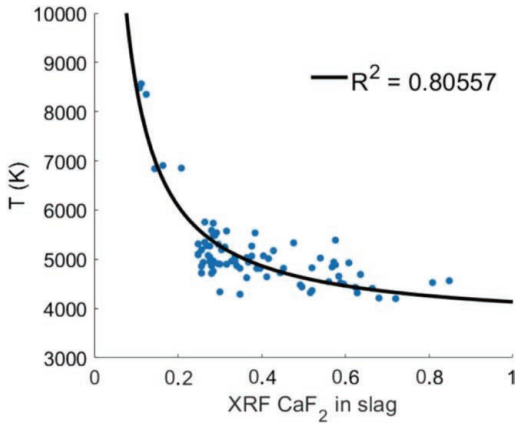

Fig. 6. Correlation between the XRF CaF_2 content in the slag and the Ca I plasma temperature derived from the VIS spectra. The correlation includes data from 78 melts. The CaF_2 content has been normalized. (Online version in color.)

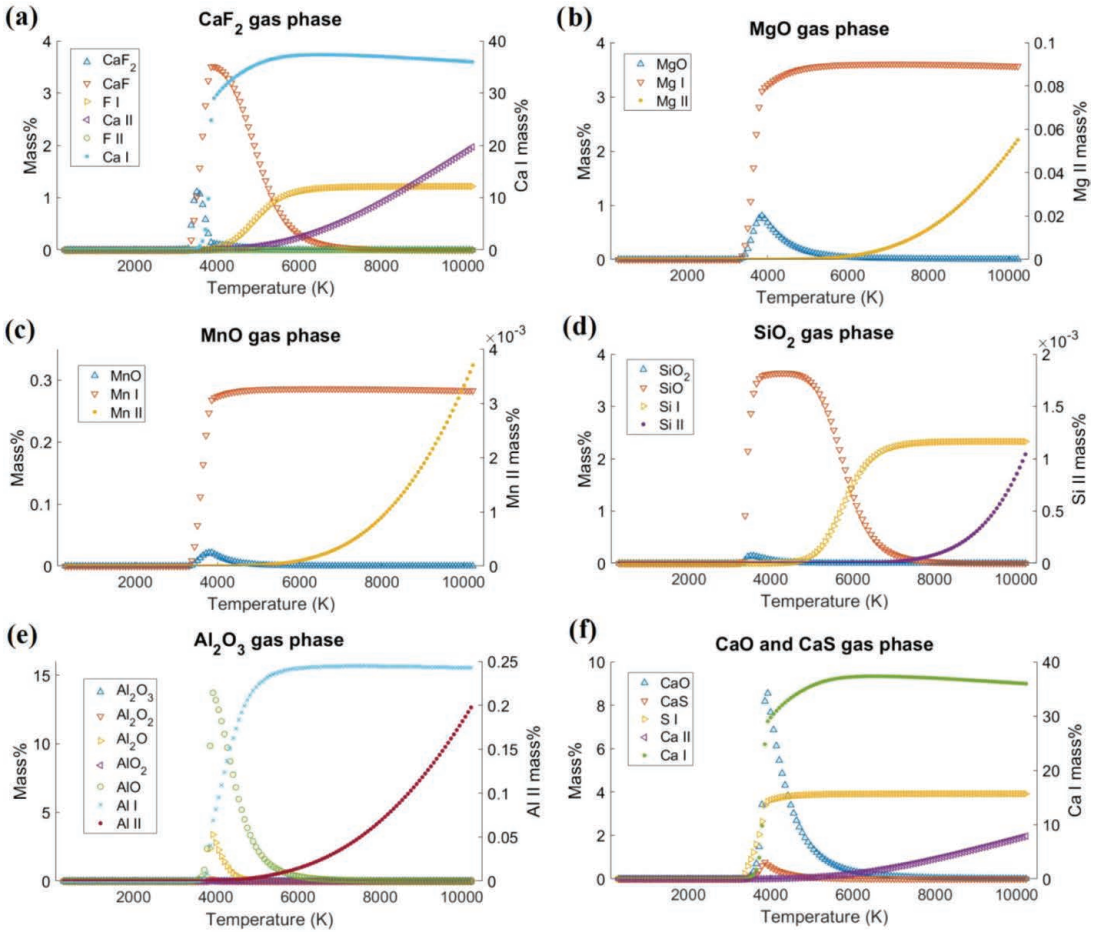

Fig. 7. Gas phases with respect to increasing plasma temperature for (a) CaF_2, (b) MgO, (c) MnO, (d) SiO_2, (e) Al_2O_3, and (f) CaO and CaS. Some neutral or ionic atomic components have been presented with the secondary y-xis on the right side if their values are very high or low, respectively. Note that the Ca I and Ca II are collective amounts from all the slag compounds that consist calcium. (Online version in color.)

$$T_{plasma} = \frac{a}{CaF_2} + b \quad \text{..... (4)}$$

According to Eq. (4), the more there is CaF_2 in the slag, the lower is the Ca I plasma temperature. This could be reasoned with higher amount of Ca I atoms in the plasma with increasing CaF_2 slag content, which might yield into self-absorption of the Ca I emission lines. This phenomenon, on the other hand, has an effect to the emission lines and thus also the plasma temperature. Thus, the actual plasma temperature might be different than what is observed using the Ca I emission lines. The R^2 values of the temperatures lower than 7 000 K are between 0.78 and 0.99, whereas above 7 000 K the R^2 drops to a range between 0.49 and 0.77 so that the lowest R^2 corresponds to the highest temperature. This indicates that the temperatures derived from the Boltzmann plot do not represent the actual plasma temperature at least above 7 000 K. However, for the purpose of this work, the link between the plasma temperatures derived with the Boltzmann plot and the CaF_2 content in the slag is more important than the actual plasma temperature. The fact that there is a correlation between the CaF_2 content of the slag and the Ca I plasma temperature means that plasma diagnostics are suitable not only for the spectrum quality evaluation but also for the slag composition analysis in the LF.

In order to better understand the relation between the slag and plasma compositions, the phase transitions of the slag components from liquid to gas were studied with HSC Chemistry software made by Outotec Oyj. The equilibrium composition analysis was carried out for CaF_2, MgO, MnO, SiO_2, CaO, CaS, and Al_2O_3 with respect to increasing temperature. Example graphs for these phase transitions have been presented in **Fig. 7** for a generic LF slag containing also traces of Cr_2O_3 and Fe_2O_3. In the Fig. 7, some of the neutral or ionic atomic components have been displayed in the secondary y-axis to the right due to very high or low values, respectively. Furthermore, the very high concentration of atomic calcium in the plasma results from all the components containing calcium, namely CaF_2, CaO, and CaS.

As can be seen from the Fig. 7, the molecular compounds of calcium, magnesium, manganese, and aluminum start to dissociate and enter the gas phase between 3 000 and 4 000 K. However, SiO is exceptionally persistent until 5 000 K, after which it starts to dissociate. Hence, the difficulty of measuring the atomic emission lines of Si I is related to the strong molecular bond of SiO. CaF and AlO are present in the plasma up to around 6 000 K, but the Ca I, F I, and Al I contents in the plasma start to increase already at 4 000 K. However, due to low amount of very intense emission lines the F I and Al I are hard to be detected. The most prominent Al I lines at 394.401 and 396.152 nm are screened by the Ca II emission lines at 393.366 and 396.847 nm. These emission lines can be distinguished from one another if the widths of the emission lines are narrow enough, which was not the case with the UV spectrometer used in this study. Also S I emission lines proved to be very hard to be identified and distinguished from the spectra, even though they are present in the plasma above 4 000 K.

Since CaF_2 and MgO have the most prominent correlations between the XRF and OES analyses together with the plasma diagnostics, the amount of Ca I, Ca II and Mg I in the plasma were studied by separately increasing either the CaF_2 or MgO content of the slag. These procedures were performed for 5 000 K and 10 000 K. The 5 000 K and 10 000 K temperatures represent the cases near the edge and the core of the plasma, respectively. The purpose of this method was to determine how the temperature affects the correlation between the slag and plasma composition for calcium and magnesium components.

The HSC Chemistry computation results for the plasma composition with respect to the slag composition are presented in **Fig. 8**. The CaF_2 and MgO contents have been normalized. Except for Ca I at 5 000 K, all the relations between the plasma and slag composition are linear. Since

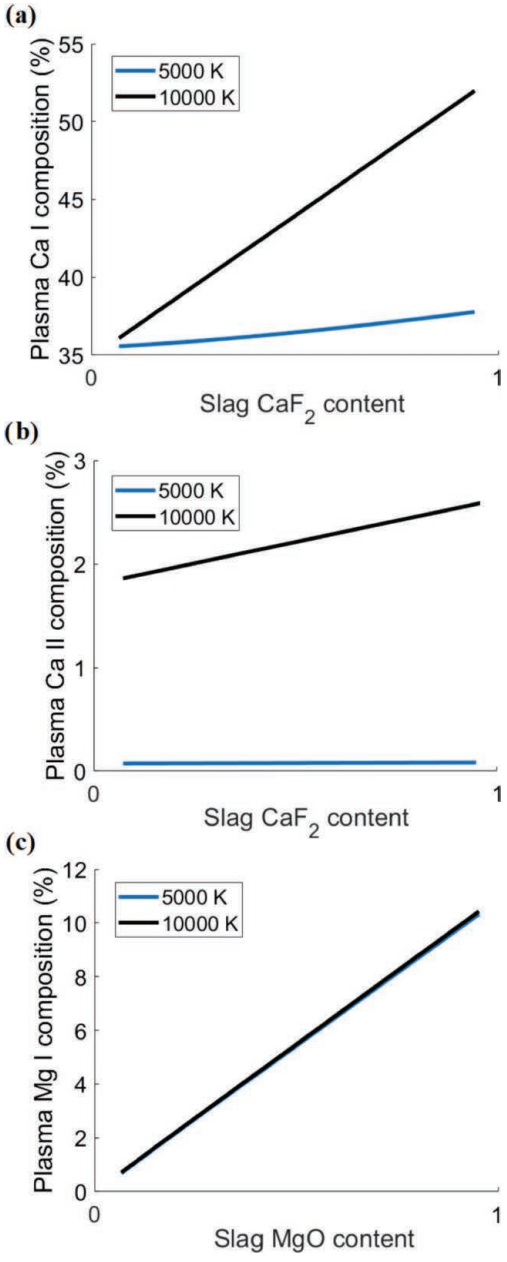

Fig. 8. Plasma composition for (a) Ca I, (b) Ca II, and (c) Mg I with respect to the slag composition for CaF_2 (a and b) and MgO (c). The CaF_2 and MgO contents have been normalized. (Online version in color.)

the plasma temperatures of EAF arcs with high R^2 have been observed to vary between the range from 4 500 to 10 000 K,[24,28] using higher plasma temperatures would be more suitable for the OES and XRF correlation analysis due to a linear relation between the plasma Ca I and slag CaF_2 composition at 10 000 K. The difference in the slope between contents of CaF_2 in the slag and Ca I in the plasma means that accurate analysis of slag composition requires understanding which of these calibration curves the observed plasma is closer.

Ca II ion concentration in the plasma is relatively low around 0.074% and increases only up to 0.085% with increasing CaF_2 slag content at 5 000 K, whereas the amount of Ca II in the plasma is notable at 10 000 K and the relation to CaF_2 slag content is more prominent. In the EAF and LF spectra, however, the Ca II emission lines are clearly observed at all plasma temperatures. The Mg I content in the plasma, on the other hand, is almost the same for both the 5 000 K and 10 000 K with only a 0.1% plasma composition difference at higher MgO slag content. The stable increase in the content of the Mg I in the plasma with respect to increasing MgO content in the slag, regardless of change in plasma temperature, emphasizes the suitability of Mg I for the emission line ratio analysis. This is supported by the intensive Mg I emission lines around 383 nm and 517 nm presented in the Table 2.

5. Conclusions

In this work, the CaF_2, MgO, and MnO contents in the slag have been evaluated with the optical emissions from the electric arc with three spectrometers. The measurement campaign was carried out in two parts, first without any additional equipment and second with a special light gathering lens. VIS and NIR spectra were analyzable without the lens, whereas the lens was required to measure the emission lines in the UV. With the UV, VIS, and NIR analyses, altogether 11 calcium, 7 magnesium, and 1 manganese lines were found to be applicable in deriving the correlation between the XRF and OES analyses. Furthermore, plasma temperature that was determined with four Ca I lines had a non-linear relation with the CaF_2 content of the slag.

The decomposition pathways of major slag components with respect to increasing plasma temperature were determined with HSC Chemistry software in order to study the dissociation pathways into their atomic and ionic components. It was noted that, except for SiO, the slag components are mostly in their atomic form already at 5 000 K. The compositions of the plasma at 5 000 or 10 000 K were studied with increasing CaF_2 or MgO contents of the slag, revealing that the composition between the slag and plasma show linear relations except between Ca I at 5 000 K and CaF_2.

Acknowledgments

This work was conducted within the Symbiosis of Metal Production and Nature (SYMMET) research program funded by Business Finland. We acknowledge the support of Research Fund for Coal and Steel under grant agreement No. 709923, Academy of Finland for Genome of Steel grant No. 311934, and Steel and Metal Producers' Fund for a 2019 postgraduate grant. We thank Luxmet Oy for the spectrometers and the OES analysis software together with Outotec Oyj for the HSC Chemistry software. We are grateful to the staff at the Deutsche Edelstahlwerke for helping with the installation of the measurement equipment.

REFERENCES

1) M. Fernandes, J. C. Pires, N. Cheung and A. Garcia: *Mater. Charact.*, **51** (2003), 301. https://doi.org/10.1016/j.matchar.2004.01.003
2) A. Rađenović, J. Malina and T. Sofilić: *Adv. Mater. Sci. Eng.*, **2013** (2013), 198240. https://doi.org/10.1155/2013/198240
3) A. N. Conejo, F. R. Lara, M. Macias-Hernández and R. D. Morales: *Steel Res. Int.*, **78** (2007), 141. https://doi.org/10.1002/srin.200705871
4) M. A. T. Andersson, P. G. Jönsson and M. Hallberg: *Ironmaking Steelmaking*, **27** (2000), 286. https://doi.org/10.1179/030192300677570
5) U. Singh, R. Anapagaddi, S. Mangal, K. A. Padmanabhan and A. K. Singh: *Metall. Mater. Trans. B*, **47** (2016), 1804. https://doi.org/10.1007/s11663-016-0620-2
6) X.-M. Yang, M. Zhang, C.-B. Shi, G.-M. Chai and J. Zhang: *Metall. Mater. Trans. B*, **43** (2012), 241. https://doi.org/10.1007/s11663-011-9612-4
7) J. H. Park, K. Y. Ko and T. S. Kim: *Metall. Mater. Trans. B*, **46** (2014), 741. https://doi.org/10.1007/s11663-014-0269-7
8) K. Y. Ko and J. H. Park: *ISIJ Int.*, **53** (2013), 958. https://doi.org/10.2355/isijinternational.53.958
9) I. Matino, V. Colla and S. Baragiola: *Waste Biomass Valoriz.*, **9** (2018), 2481. https://doi.org/10.1007/s12649-018-0264-3
10) A. S.-d.-G. Vilaplana, V. J. Ferreira, A. M. López-Sabirón, A. Aranda-Usón, C. Lausín-González, C. Berganza-Conde and G. Ferreira: *Constr. Build. Mater.*, **94** (2015), 837. https://doi.org/10.1016/j.conbuildmat.2015.07.075
11) Y. Jiang, T.-C. Ling, C. Shi and S.-Y. Pan: *Resour. Conserv. Recycl.*, **136** (2018), 187. https://doi.org/10.1016/j.resconrec.2018.04.023
12) V. Z. Serjun, B. Mirtič and A. Mladenovič: *Mater. Technol.*, **47** (2013), No. 5, 543.
13) I. Liapis and I. Papayianni: *J. Hazard. Mater.*, **283** (2015), 89. https://doi.org/10.1016/j.jhazmat.2014.08.072
14) A. Picon, A. Vicente, S. Rodriguez-Vaamonde, J. Armentia, J. A. Arteche and I. Macaya: *IEEE Trans. Ind. Inform.*, **14** (2018), 3506. https://doi.org/10.1109/TII.2017.2773068
15) A. Harada, N. Maruoka, H. Shibata and S. Kitamura: *ISIJ Int.*, **53** (2013), 2110. https://doi.org/10.2355/isijinternational.53.2110
16) A. Harada, N. Maruoka, H. Shibata and S. Kitamura: *ISIJ Int.*, **53** (2013), 2118. https://doi.org/10.2355/isijinternational.53.2118
17) C. Behera and U. K. Mohanty: *ISIJ Int.*, **41** (2001), 834. https://doi.org/10.2355/isijinternational.41.834
18) J. H. Park, D. J. Min and H. S. Song: *Metall. Mater. Trans. B*, **33** (2002), 723. https://doi.org/10.1007/s11663-002-0026-1
19) F. Shahbazian: *Scand. J. Metall.*, **30** (2001), 302. https://doi.org/10.1034/j.1600-0692.2001.300505.x
20) L. Wu, J. Gran and D. Sichen: *Metall. Mater. Trans. B*, **42** (2011), 928. https://doi.org/10.1007/s11663-011-9546-x
21) Y. Taniguchi, K. Morita and N. Sano: *ISIJ Int.*, **37** (1997), 956. https://doi.org/10.2355/isijinternational.37.956
22) Y. N. Jia, L. G. Zhu, C. J. Zhang and P. Pei: *Ironmaking Steelmaking*, **44** (2017), 796. https://doi.org/10.1080/03019233.2016.1240848
23) M. Aula, T. Demus, T. Echterhof, M. Huttula, H. Pfeifer and T. Fabritius: *ISIJ Int.*, **57** (2017), 478. https://doi.org/10.2355/isijinternational.ISIJINT-2015-677
24) M. Aula, A. Leppänen, J. Roininen, E.-P. Heikkinen, K. Vallo, T. Fabritius and M. Huttula: *Metall. Mater. Trans. B*, **45** (2014), 839. https://doi.org/10.1007/s11663-014-0032-0
25) C. Aragón and J. A. Aguilera: *Spectrochim. Acta Part B*, **63** (2008), 893. https://doi.org/10.1016/j.sab.2008.05.010
26) R. W. P. McWhirter: Plasma Diagnostic Techniques, Chapter 5, ed. by R. H. Huddlestone and S. L. Leonard, Academic Press, New York, (1965), 201.
27) A. Kramida, Y. Ralchenko, J. Reader and NIST ASD Team: NIST Atomic Spectra Database, https://doi.org/10.18434/T4W30F, (accessed 2019-08-22).
28) H. Pauna, T. Willms, M. Aula, T. Echterhof, M. Huttula and T. Fabritius: *Plasma Res. Express*, **1** (2019), 035007. https://doi.org/10.1088/2516-1067/ab30dd